Two-component aerosol dynamic simulation using differentially weighted operator splitting Monte Carlo method

HM Liu[1] and TL Chan[1,2]*

[1]Department of Mechanical Engineering, The Hong Kong Polytechnic University, Kowloon, Hong Kong

[2]The Hong Kong Polytechnic University, Shenzhen Research Institute, Shenzhen, P.R. China

*Corresponding author and E-mail address: mmtlchan@polyu.edu.hk (T.L. Chan)

Abstract

A differentially weighted operator splitting Monte Carlo (DWOSMC) method is further developed to study multi-component aerosol dynamics. The proposed method involves the use of an excellent combination of stochastic and deterministic approaches. Component-related particle volume density distributions are examined, and the computational accuracy and efficiency of the two-component DWOSMC method is verified against a sectional method. For the one-component aerosol system, the sectional method is more computationally efficient than the DWOSMC method, while for two-component aerosol systems, the DWOSMC method proves to be much more computationally efficient than the sectional method. Using this newly modified DWOSMC method, compositional distributions of particles can be obtained to determine simultaneous coagulation and condensation processes that occur in different regimes of two-component aerosol systems.

Keywords: Differentially weighted operator splitting Monte Carlo, multi-component, aerosol dynamics, compositional distribution, computational efficiency

Nomenclature

A, B	component symbol
$A_0(t)$	analytical value
$A(t)$	numerical simulation value
C_i	coagulation rate of simulation particle, i
d	particle diameter (m)
i, j	particle label
I	condensation kernel (m^3/s)
K	coagulation kernel (m^3/s)
k_B	Boltzmann constant (J/K)
M	prescribed number of Monte Carlo loops
$n(t)$	number density of aerosol particles
N	particle number concentration during the simulation interval
N_0	initial particle number concentration
N_r	number of real particles
N_s	number of simulation particles
P_i	probability of coagulation event taking place on particle i
$q_{0,0}$	particle number distribution
$q_{1,0}$, $q_{0,1}$	component-related particle volume density distribution
r_1, r_2	random number
t	simulation time (s)
T_K	temperature (K)
Δt	time-step (s)
δt	time-step (s)
v, v'	particle volume (m^3)

V	total particle volume during the simulation interval (m^3)
V_0	initial total volume of aerosol particles (m^3)
V_s	the volume of the aerosol simulation system (m^3)
w_i	weight of simulation particle, i
X	total process
X_1, X_2	sub-processes

Subscripts

A,B	component symbol
coag	coagulation
cond	condensation
i, j, m, n	index of simulation particles

Superscripts

a, b	particle moments index
k	particle section index

Greek letters

α	correction factor
ε	relative error
ρ	particle density
τ	normalized computation time in Eq. (20)
$\sigma_1, \sigma_A, \sigma_B$	condensation kernel factor
σ	standard deviation of the normal distribution
ξ	particle volume density

Abbreviations

DSMC   direct simulation Monte Carlo

DWOSMC   differentially weighted operator splitting Monte Carlo

GDE   general dynamics equation

MC   Monte Carlo

MOM   method of moment

PBE   population balance equation

PSD   particle size distribution

SM   sectional method

1 Introduction

Aerosols are essentially multivariate fine particulates involving complex chemical reactions and compositions. The dynamic behaviors of aerosol particles are related to many engineering and scientific applications and problems such as the natural phenomenon of acid rain formation and deposition [1], combustion particulate emissions that can directly affect human health [2], silica and titania nanoparticle flame synthesis in pigments and catalysts [3], etc. In these fields, particles often consist of multiple components and compositional inhomogeneities, and particle size and compositional distributions affect the properties of particles. The interaction effects of aerosol chemical compositions and particle properties on the atmosphere, climates and human health are very important in atmospheric and environmental research [4]. Particle compositions affect the scope and scale of climatic forces. Such particles can play significant role in the Earth's energy balance by taking in and scattering incoming solar radiation, and outgoing thermal radiation [5]. Therefore, air pollution, global climate change and the behaviors of atmospheric aerosol particles have increasingly attracted the attention of scientists. A complete and scientific understanding of particle component compositions, chemical interactions and transformations is required for the effective control of aerosol effects on the global climate and human health. For spatially homogeneous aerosols, particles are mostly characterized by their sizes, concentrations and chemical compositions, and so it is inevitable for multi-component particles to be considered in the study of aerosols [6]. The particle size distribution is affected by several physical and chemical phenomena such as those of nucleation, coagulation, condensation, deposition, breakage, etc. [7–10]. For atmospheric aerosols, coagulation and condensation are the most important processes, as many of the properties of aerosols (light scattering, radioactivity and capturing strategies) are dependent on the size and compositional distributions of particles. Furthermore, coagulation and condensation processes are very important phenomena to the evolution of particle sizes and compositional distributions [11–13]. Therefore, these two processes have been widely explored in studies on particle size and compositional distributions.

Dynamics of particle growth are typically described by the population balance equation (PBE) [14], which is also known as the general dynamic equation (GDE) [15]. The GDE describing simultaneous coagulation and condensation processes is expressed as

$$\frac{\partial n(v,t)}{\partial t} = \frac{1}{2}\int_0^v K(v-v',v')n(v')n(v-v')\mathrm{d}v' - \int_0^\infty K(v,v')n(v)n(v')\mathrm{d}v' - \frac{\partial(I_0 n)}{\partial v}(v,t) \tag{1}$$

where n is the number concentration of particles with a volume v, the coagulation kernel $K(v,v')$ is the rate of particles with a volume v coagulating with particles with a volume v'. The condensation rate $I_0(v,t)$ is typically related to the surface area of particles. The term shown on the left side of Eq. (1) describes the evolution of the number density of particles with volume v. The first two terms on the right side denote the particle number density variations resulting from coagulation processes, and the third term on the right side denotes particle number density variations attributable to condensation.

5

Over the past several decades, considerable efforts have been made to numerically solve the aerosol GDE, and most of these efforts have been devoted to solving one-component aerosol processes [16,17,12,18,19]. Other researchers have focused on multi-component aerosol processes. Gelbard and Seinfeld [6] developed a sectional method for simulating variations in aerosol particle size and compositional distributions for coagulation, chemical reaction and growth processes. Later on, Gelbard [20] developed a moving-sectional method for modeling multi-component condensation. Kim and Seinfeld successively proposed a moving sectional method [21], a numerical technique coupling repeated upwind difference method (RUD) and the Taylor-Galerkin method (TGFEM) [22] to obtain the multivariable size-composition distributions of aerosol systems based on simultaneously occurring coagulation and condensation processes. Katoshevski and Seinfeld [23] first developed an analytical solution for multi-component aerosol dynamics based on particle condensation/evaporation. Based on this method, Katoshevski and Seinfeld [24] further proposed an analytical-numerical method for the solution of multi-component aerosol GDE accounting for growth, removal, particle sources, and coagulation. Sun et al. [25,26] sequentially used the sectional and Monte Carlo methods to simulate two-component aerosol dynamics including coagulation and condensation processes. Korhonen et al. [5] introduced a size-segregated multi-component aerosol dynamics model for the investigation of tropospheric layer aerosol particles. Matsoukas et al. [27], Efendiev [28], and Zhao and Zheng [29] simulated the two-component coagulation of different kernels using the Monte Carlo method. Matsoukas et al. [30] introduced the aggregative mixing degree, which can influence particle size and compositional distributions. Later, Lee et al. [31] demonstrated that the steady-state mixing degree is the single parameter to determine the width of the compositional distribution in bicomponent aggregation systems. Zhao et al. [32,33], and Zhao and Kruis [34] further studied the evolution of the aggregative mixing degree for different aggregation regimes and initial conditions of two-component aggregation. Palaniswaamy [35] used the direct simulation Monte Carlo (DSMC) method to investigate multi-component aerosol dynamics of coagulation, deposition, growth, and source reinforcement. Fu et al. [13] developed a finite element method for solving multi-component aerosol dynamic equations based on processes of coagulation and condensation.

For a two-component aerosol system that only considers coagulation and condensation processes, the governing equation becomes [29,36],

$$
\frac{\partial n(v_A,v_B,t)}{\partial t} = \frac{1}{2}\int_0^{v_A}\int_0^{v_B} K(v_A - v_A',v_B - v_B',v_A',v_B', t)\, n(v_A - v_A',v_B - v_B', t)n(v_A',v_B', t)\mathrm{d}v_A'\mathrm{d}v_B'
$$

$$
- n(v_A,v_B,t)\int_0^{\infty}\int_0^{\infty} K(v_A,v_B,v_A',v_B', t)n(v_A',v_B', t)\mathrm{d}v_A'\mathrm{d}v_B' - \frac{\partial(I_A n)}{\partial v_A}(v_A,v_B,t) \qquad (2)
$$

$$
- \frac{\partial(I_B n)}{\partial v_B}(v_A,v_B,t)
$$

where v_A and v_B are the volume of A-component and B-component within a particle with a total

volume of v_A+v_B, respectively; $n(v_A,v_B,t)$ is the number density of particles with a volume of v_A+v_B at time t such that $n(v_A,v_B,t)\mathrm{d}v_A\mathrm{d}v_B$ denotes the number concentration of particles in the size range of A-component v_A to $v_A+\mathrm{d}v_A$, and the size range of B-component v_B to $v_B+\mathrm{d}v_B$; $K(v_A,v_B,v_A',v_B',t)$ is the coagulation kernel between one particle of volume (v_A,v_B) and another particle of volume (v_A',v_B'). The coagulation of two particles results in the production of a new two-component particle with a volume of (v_A+v_A', v_B+v_B') and the destruction of two previous particles. I_A and I_B are the condensation rate coefficients of the A-component and B-component, respectively. The occurrence of a condensation event either in the A-component or the B-component would vary (either an increase or decrease depending on the derivative of the condensation rate with particle volume) the number density of particles of state (v_A, v_B) as expressed in Eq. (2).

The double integral and nonlinear features of Eq. (2) render it difficult to solve. Conventional numerical methods for solving the GDE of aerosols are classified as two types of mathematical models: deterministic and stochastic models. Deterministic models mainly include the sectional method (SM) [8] and method of moments (MOM) [37–40], which are comparatively efficient at solving the GDE of mono-variant systems. The stochastic model typically refers to the Lagrangian Monte Carlo method. Compared to deterministic methods, a major shortcoming of the Monte Carlo (MC) method relates to its computational time and computer memory usage. However, in addressing multicomponent problems, the MC method is more worthy of consideration in that considering more than one component does not add considerable complexity to the arithmetic programming [25]. On the other hand, for the deterministic method, considering more components inevitably increases the complexity of the algorithm while enhancing innate fluctuations and numerical diffusion [29].

Monte Carlo simulations are able to capture the history, trajectory, particle size distribution and multi-variate information of aerosol particles. They are robust and straightforward in addressing stochastic processes. The MC method was originally proposed by [41] and applies laws of probability to the natural sciences. It was then developed to simulate rarefied gas flows problems [42,43] and dispersed particle related problems [16]. Unlike deterministic methods, it does not directly solve the GDE for aerosol dynamics, as it instead uses numerical particles to simulate the behaviors of real particles. For this reason, the MC method can solve aerosol dynamics problems from several random samplings drawn from the particle system. The discrete and probabilistic nature of the MC method renders it ideally suitable for addressing particle dynamics of the same nature [44]. Furthermore, every numerical particle has its own size, composition and morphology, and the use of more component dimensions does not significantly increase the complexity of the algorithm [45]. Thus, compared to other methods, MC methods are increasingly being used to manage multivariate and polydispersed systems.

Compared to deterministic methods, such as SMs and MOMs, one disadvantage of traditional MC methods relates to conflicts between the computational accuracy and efficiency owing to their stochastic and statistical characteristics. Both the computational accuracy and efficiency are highly related to the number of simulation particles used in MC methods. When high levels of computational accuracy are required, considerable computer memory and computational time requirements apply [16]. However, with the rapid development of computer technologies, computers with more memory space and that operate at faster speeds are being developed, and the computational costs (i.e., memory and time consumption) of MC methods are thus no longer a major issue. Furthermore, "weighted simulation particles" [46,47] are widely used in MC methods due to the large number of real particles in systems simulated. To further overcome issues related to computational costs and accuracy levels, Zhao et al. [48] developed a differentially weighted Monte Carlo (DWMC) method that proved to be quite efficient and effective at simulating aerosol coagulation, and then the DWMC method was further used to investigate the two-component coagulation of aerosol dynamics systems. On the other hand, the deterministic method tends to be more efficient at simulating aerosol condensation and nucleation processes, and for simulating gas phase flows. Celnik et al. [49] and Menz et al. [50] accomplished the full-coupling of soot particles with the gas phase using the operator splitting technique where the soot particles are simulated using the Monte Carlo method and the gas phase is solved using an implicit ordinary differential equation (ODE) solution accordingly. Zhou et al. [17] and Liu and Chan [18] also recently used the operator splitting technique to couple the stochastic Monte Carlo method with deterministic methods for aerosol dynamics. Recently, Liu and Chan [51,52] proposed a differentially weighted operator splitting Monte Carlo (DWOSMC) method that couples the operator splitting technique with the differentially weighted Monte Carlo method to efficiently examine complex dynamic behaviors of aerosols including those of nucleation, coagulation, condensation, etc. In the present study, the newly developed DWOSMC method is further extended to simulate multi-component aerosol dynamic processes in which only coagulation and condensation processes are considered owing to their significance for the evolution of particle size and compositional distributions. The method is proven capable of capturing composition and size distributions and bivariate compositional distributions of aerosols. As no explicit solutions for two-component complex aerosol systems are available, the two-component DWOSMC method is initially verified by a sectional method, and the computation efficiency levels of the two methods are compared based on one- and two-component aerosol simulation systems.

2 Mathematical model

In our previous study [52], a differentially weighted operator splitting Monte Carlo (DWOSMC) method was proposed for one-component aerosol systems by using the operator splitting technique to combine stochastic MC and deterministic integration methods. In the present study, the DWOSMC method is further developed to simulate multi-component aerosol systems. A brief outline of the

algorithm's application to two-component systems is given as follows:

(a) Start M Monte Carlo loops.

(b) Initialization. The initial value of particle properties (size, weight, number concentration, component composition, etc.) is first assigned according to an initial compositional distribution. During the simulation of the DWOSMC method, the weights of different simulation particles can differ. For a two-component aerosol system, w_i is defined as,

$$w_i = \frac{N_r(v_A, v_B)}{N_s(v_A, v_B)} \tag{3}$$

where $N_r(v_A, v_B)$ is the number of real particles of A-component volume size v_A and B-component volume size v_B, and where $N_s(v_A, v_B)$ is the number of simulation particles representing these real particles $N_r(v_A, v_B)$. In the present study, the weights of all simulation particles are set to the same value $w_{i,0}$ at the time of initialization. The initial size v_0 and number density distributions $n(v_A, v_B, 0)$ of the particles are set according to the initial distributions assigned.

(c) Choose a time step δt. A variable time scale is determined by different aerosol dynamic processes. Specifically, the characteristic time scale used for coagulation events is written as:

$$\Delta t_{coag} = \min|_{\forall i} (V_s / \sum_{j=1, j\neq i}^{N_s} K'_{ij}) \tag{4}$$

where V_s and N_s are the volume of the aerosol simulation system and the total number of simulation particles, respectively. K'_{ij} is the normalized coagulation kernel for simulation particles i and j. K'_{ij} is not only related to the size or state of particles but is also related to the weights of the two coagulated particles:

$$K'_{ij} = 2K_{ij}w_j \max(w_i, w_j)/(w_i + w_j)$$

where K_{ij} is the coagulation kernel of particles i and j.

For condensation events, the characteristic time scale is written as:

$$\Delta t_{cond} = \min|_{\forall i} (v_i / I_0(v)) \tag{5}$$

where v_i is the volume of particle i and where $I_0(v)$ is the condensation kernel.

To guarantee the accuracy of the proposed method in simulating both condensation and coagulation processes, an appropriate time step that is smaller than both characteristic time scales of the two events should be used. In the present study, the time step is written as:

$$\delta t = \alpha \min(\Delta t_{coag}, \Delta t_{cond}) \tag{6}$$

where α is an empirical parameter set as 0.01 [53,54] during calculation to ensure that an accurate integration of aerosol dynamic processes is achieved.

(d) Integration. Stochastic and deterministic aerosol dynamic processes are managed by applying the second-order Strang splitting method which is expressed as:

$$\exp(\delta t X) = \exp\left(\frac{1}{2}\delta t X_2\right)\exp(\delta t X_1)\exp\left(\frac{1}{2}\delta t X_2\right) + \mathcal{O}\left(\delta t^3\right) \tag{7}$$

where X is the total process of two sub-processes, X_1 refers to the coagulation process, and X_2 refers to the condensation process.

Within the time step, the condensation process is first calculated for the first half time-step of $\delta t/2$, and then the coagulation process is simulated for one time-step δt. Finally, the condensation process is calculated for the last half time-step of $\delta t/2$. The integration procedure used for the total process of the two sub-processes for one time-step is described in steps (e) to (g).

(e) Integration of condensation for a time-step of $\delta t/2$.

The condensation event affects the particle size distribution of aerosols because it produces larger particles. In two-component systems, there are two condensation kernels (i.e., one for component A and one for component B) written as $I_A(v_A)$ and $I_B(v_B)$, respectively. In the present study, all particles are assumed to be spherical and that the volume of particles is the sum of their two components after the condensation event, which is written as,

$$\frac{dv_i(v_A, v_B, t)}{dt} = I_A(v_A) + I_B(v_B) \tag{8}$$

Specifically in the present study, within a time-step of $\delta t/2$, the condensation event is calculated as:

$$v_i' = v_i + (I_A(v_A) + I_B(v_B))\delta t/2 \tag{9}$$

$$w_i' = w_i \tag{10}$$

where w_i and v_i refer to the weight and volume of simulation particle i, respectively, before the condensation event and w_i', and v_i' refer to the weight and volume of simulation particle i, respectively, after the condensation event.

(f) Integration of coagulation for a time-step of δt.

The simulation of coagulation is based on the DWMC method proposed by Zhao et al. [48,53]. The occurrence of coagulation events between two particles is based on probability selections. During simulation, the probability of coagulation events taking place in particle i within δt is calculated as:

$$P_i = 1 - \exp(-V_s C_i \delta t/2) \tag{11}$$

where V_s is the volume of the simulation system and C_i is the coagulation rate of simulation particle i based on the probabilistic coagulation rule written as:

$$C_i = \frac{1}{V_s^2} \sum_{j=1,j\neq i}^{N_s} K'_{ij} \tag{12}$$

where N_s is the simulation particle number and K'_{ij} is the normalized coagulation rate for particles i and j:

$$K'_{ij} = 2K_{ij}w_j\max(w_i,w_j)/(w_i+w_j) \tag{13}$$

Particle i is selected as the first coagulation particle when P_i satisfies,

$$r_1 \leq P_i \tag{14}$$

where r_1 is a random number of between 0 and 1 generated from a uniform distribution.

A second coagulation particle j is selected when Eq. (15) is satisfied, and then the coagulation event is managed between particles i and j; otherwise the remaining particles are checked until the second particle j is selected.

$$r_2 \leq K'_{ij}/\max(K'_{mn})|_{\forall m, \forall n} \tag{15}$$

where r_2 is a number of between 0 and 1 randomly generated from a uniform distribution.

After the coagulation event, the previous particles are replaced with two newly weighted simulation particles, and the conservation of volume is considered while the properties of these particles are changed. The coagulation process is described as [29]:

$$\text{If} \quad w_i=w_j, \begin{cases} w'_i=w_i/2; \; v'_i=v_i+v_j, \; v'_{i,A}=v_{i,A}+v_{j,A}, \; v'_{i,B}=v_{i,B}+v_{j,B}; \\ w'_j=w_j/2; \; v'_j=v_i+v_j; \; v'_{j,A}=v_{i,A}+v_{j,A}, \; v'_{j,B}=v_{i,B}+v_{j,B}; \end{cases} \tag{16a}$$

$$\text{If} \quad w_i \neq w_j, \begin{cases} w'_i=\max(w_i,w_j)-\min(w_i,w_j); v'_i=v_m|_{w_m=\max(w_i,w_j)}; \\ v'_{i,A}=v_{m,A}|_{w_m=\max(w_i,w_j)}, \; v'_{i,B}=v_{m,B}|_{w_m=\max(w_i,w_j)}; \\ w'_j=\min(w_i,w_j); v'_j=v_i+v_j; \\ v'_{j,A}=v_{i,A}+v_{j,A}, \; v'_{j,B}=v_{i,B}+v_{j,B}; \end{cases} \tag{16b}$$

where w'_i, w'_j, v'_i and v'_j represent the weight or volume of newly created simulation particles i and j after the coagulation event. $v'_{i,A}$, $v'_{i,B}$, $v'_{j,A}$ and $v'_{j,B}$ are the volumes of components A and B in newly created simulation particles i and j after the coagulation event. In the present study, the density of particles is assumed to be constant, and so the conservation of particle volumes in Eq. (16) denotes the conservation of mass during the coagulation event.

(g) Condensation is integrated for a time-step of $\delta t/2$. The calculation procedure is the same as that used in step (e).

(h) The properties of simulation particles are updated to obtain information (size, composition and number density, etc.) on the particles, as the particles are assumed to be spherical before and after coagulation and condensation events, and thus particle diameters can be easily derived.

(i) Repeat steps (c) to (h) until the predetermined stopping time t_{stop} is reached, and then exit the current Monte Carlo loop.

(j) Start a new Monte Carlo loop if calculated Monte Carlo loop number R is smaller than predetermined Monte Carlo loop number M. Otherwise the averaged results are obtained to output the information of the aerosol system. In the present study, eight Monte Carlo loops are carried out.

Fig. 1 presents a flowchart of the full algorithm of the two-component DWOSMC method.

Fig. 1   Flowchart of the two-component DWOSMC algorithm.

3   Results and Discussion

In the present study, the performance of the multi-component DWOSMC method is evaluated using a sectional method [8], which is also further developed according to Kim and Seinfeld's [21] concept of a moving sectional method that describes the two-component system. First, the DWOSMC and sectional methods are evaluated in a simple one-component case for which analytical solutions exist. Then, two-component systems with different kernels and initial particle size distributions are examined to determine the capacity for the multi-component DWOSMC method to simulate aerosol dynamics. In the present study, different cases are successively investigated to study simultaneous coagulation and condensation processes. For the sectional method, particles only exist at discretized nodes, and the aerosol size spectrum is divided into 50~70 sections. The same number of nodes is also used for the DWOSMC method to store the particle size and compositional distributions of aerosols. In our previous study [52], the impact of the number of simulation particles on the computational efficiency and accuracy of the DWOSMC method is examined. Herein, unless otherwise stated, the present simulations are performed on 4000 simulation particles.

3.1   One-component coagulation and condensation case

In the present study, this developed multi-component DWOSMC method is firstly used to calculate a one-component aerosol system by setting the growth kernels of components A and B to be the same. The results are verified by analytical solutions, and compared with the sectional method [8,21] and a non-weighted direct simulation Monte Carlo (DSMC) method [56] to evaluate the computational efficiency and accuracy of this DWOSMC method.

For a one-component aerosol system, constant kernel coagulation and linear kernel condensation are considered in Case I. Particles are initially uniformly distributed, the initial total particle number

concentration is $N_0 = 10^5/\text{m}^3$, and the initial average particle volume is $v_0 = 1\times10^{-22}$ m^3. Analytical solutions for dimensionless particle number concentration $N(t)/N_0$, and total particle volume concentration $V(t)/V_0$ are given by [11],

$$N(t)/N_0 = \frac{1}{1 + K_0 N_0 t/2} \tag{17}$$

$$V(t)/V_0 = \exp(\sigma_1 t) \tag{18}$$

In Case I, the constant coagulation kernel is $K = K_0$ where $K_0 = 5\times10^{-6}$ m^3/s, and the linear condensation kernel is $I = \sigma_1 v$, $\sigma_1 = 2\times10^{-2}$/s [55]. Numerical simulation time t_{stop} is taken as 200 s.

Fig. 2　Time evolution of (a) dimensionless particle number concentration N/N_0 and total particle volume V/V_0 ; and (b) the relative error ε (%) for N/N_0 obtained from the SM, DWOSMC and DSMC methods, and the corresponding normalized computation time τ, for Case I.

Fig. 2(a) shows the time evolution of dimensionless particle number concentration N/N_0 and total particle volume V/V_0. For simultaneously occurring coagulation and condensation processes, the particle number density level decreases over time due to the coagulation event, and the total particle volume increases over time due to the condensation process. As was expected, excellent matches are found from the SM, DWOSMC and DSMC methods and from the analytical solutions.

The computational accuracy and efficiency of the three methods are then examined further. The relative error ε (%) of the particle number concentration and normalized computational time τ are shown in Fig. 2(b). The relative error ε and normalized computational time τ are respectively, defined by the following equations.

$$\varepsilon = |A(t)-A_0(t)|/A_0(t) \tag{19}$$

$$\tau = t/t_{\text{SM}} \tag{20}$$

where $A_0(t)$ is the value obtained from the analytical solution, where $A(t)$ is the value obtained from the three corresponding methods (i.e., SM, DWOSMC, and DSMC), where t_{SM} is the computation time required for SM, and where t is the amount of computing time required for corresponding methods (SM, DWOSMC, and DSMC).

In Fig. 2 (b) the relative errors ε obtained from the three methods are quite small and are mostly less than 1%. On the other hand, it is observed that the relative error obtained from the DSMC is greater than that derived from the SM and DWOSMC. Furthermore, much less computation time is required for the DWOSMC than for the DSMC, proving that the DWOSMC is much more computationally accurate and efficient than the DSMC. Furthermore, the relative error obtained from

the SM is extremely small at less than 0.2% for the whole numerical simulation for Case I. As the SM closely reflects the analytical solution shown in Figs. 2(a) and (b), it is used to verify the proposed two-component DWOSMC method in the present study.

The particle number distributions are examined for Case I as shown in Fig. 3, which shows that initially uniform distributed particles evolve into a normal distribution over time. Satisfactory agreement is found between the SM and Monte Carlo methods.

Fig. 3 Evolution of particle number distributions obtained from the sectional (solid line), DWOSMC (scattered solid points) and DSMC (scattered unshaded points) methods for Case I.

3.2 Two-component coagulation and condensation process and constant coagulation kernel cases

For a multi-component aerosol system, the component-related volume density of particles is of interest. The total volume density of a particle is defined as [57,58],

$$\xi(v,t) = vn(v,t) \tag{21}$$

The i-th component related volume density of particle of volume v is

$$\xi_i(v,t) = v_i(v,t)n(v,t) \tag{22}$$

Specifically, for a two-component system, $\xi_A(v,t)$ and $\xi_B(v,t)$ are the volume density values of the A-component and B-component, respectively, and then $\xi(v,t)=\xi_A(v,t)+\xi_B(v,t)$.

When particles are divided into multiple sections by size, the component-related volume density of $v_{l,k} < v_k < v_{u,k}$ in size in the k-th section is

$$q_{a,b}^k(t) = \int_{v_{l,k}}^{v_{u,k}} v_A^a(v,t)v_B^b(v,t)n(v,t)\mathrm{d}v \qquad (0 \leq a,b \leq 1) \tag{23}$$

where $v_{l,k}$ and $v_{u,k}$ are the lower and upper bounds of the volumes of particles in the k-th section, respectively and $v = v_A+v_B$. Specifically, $q_{0,0}^k$ is the particle number concentration of the k-th section. $q_{1,0}^k$, and $q_{0,1}^k$ are the particle volume densities of components A and B in the k-th section, respectively.

In the following studied cases, the component-related volume densities of particles are presented in all particle volume sections where the particle volume is converted into a particle diameter as an

14

independent variable. Therefore, $q_{0,0}$ is the particle number distribution and $q_{1,0}$ and $q_{0,1}$ are the particle volume density distributions of components A and B, respectively.

3.2.1 Initially uniformly distributed and compositionally equal volume case

The initial particle size distribution is considered to be uniform for Case II. The initial total particle number is $N_0 = 10^5/m^3$, and the initial average particle volume is $v_0 = 1 \times 10^{-22}$ m³ and consists of particles with equal volumes of components A and B. The constant coagulation kernel is given by $K_0 = 5 \times 10^{-6}$ m³/s, and linear condensation kernels for components A and B are given by $I_A = \sigma_A v_A$, $\sigma_A = 1 \times 10^{-3}/s$, and $I_B = \sigma_B v_B, \sigma_B = 2 \times 10^{-3}/s$, respectively. A numerical simulation time of 200 s is used.

Fig. 4 shows the time evolution of the dimensionless particle number concentration N/N_0 and total particle volume V/V_0 as well as the particle number distribution for simulation times t of 20, 60, 100 and 200 s. In Fig. 4(a), the particle number concentration and total particle volume obtained by using the DWOSMC method are in excellent agreement with those derived from the SM. In Fig. 4(b), as the initial particle diameter is uniform and small, when the simulation time is 20 s, the particle number density of small diameters is quite large. In addition, as simulation time advances, both coagulation and condensation events take place, and the particle number distribution evolves to a normal distribution after 100 s and 200 s of simulation time. From Figs. 4(a) and (b), the results of the DWOSMC method coincide with those derived from the SM.

Fig. 4   Time evolutions of (a) N/N_0 and V/V_0 and (b) particle number distributions obtained from the SM (solid line) and DWOSMC method (scattered solid points) for Case II.

The time evolutions of particle volume density distributions of components A and B for Case II are shown in Figs. 5(a) and 5(b), respectively. It is shown that the variation tendencies of particle volume density distributions for components A and B are quite similar over time while the peak value of $q_{1,0}$, and $q_{0,1}$ moves along the larger diameter d. This occurs because both coagulation and condensation processes generate a larger average particle diameter. From Fig. 5 (a) and (b), the results obtained from the DWOSMC agree well with those of the SM. Hence, the DWOSMC method can predict two-component particle volume distributions for constant coagulation kernels and linear condensation kernels.

Fig. 5   Time evolutions of particle volume density distributions of (a) A-component and (b) B-component obtained from the SM (solid line) and DWOSMC method (scattered solid points) for Case II.

3.2.2 Initially uniformly distributed and compositionally different volume case

The initial particle size distribution is considered to be uniform while the compositions of components A and B are different for Case III. The initial total particle number is $N_0 = 10^5/m^3$ and the

initial average particle volume is $v_0=1\times10^{-22}$ m^3, in which the volumes of components A and B are v_{A0} = $v_0/3$ and $v_{B0}= 2v_0/3$, respectively. Coagulation and condensation kernels are the same as those used for Case II. A simulation period of 200 s is used.

Fig. 6   Time evolution of (a) N/N_0 and V/V_0 and (b) particle number distributions obtained from the SM (solid line) and DWOSMC method (scattered solid points) for Case III.

The time evolution of dimensionless particle number density N/N_0 and total particle volume V/V_0, as well as the particle diameter distribution of $q_{0,0}$ for simulation times 60 s and 200 s for Case III are shown in Fig. 6. For N/N_0 and V/V_0, results obtained from the SM and DWOSMC method show excellent agreement with one another. For $q_{0,0}$, the distribution of $q_{0,0}$ suffers fluctuations when the simulation time is 60 s, and fluctuations resulting from the DWOSMC method tend to be greater than those of the SM, but the distribution curve for these two methods share the same patterns. The distribution of $q_{0,0}$ is normal when the simulation period reaches 200 s, and results obtained from the DWOSMC method and SM agree well with one another.

Fig. 7 shows the particle volume density distributions of components A and B for different simulation periods (60 s and 200 s). From Fig. 7 (a), while the distribution trends of the two methods are similar for a simulation time of 60 s, some fluctuations result from the DWOSMC method. While such fluctuations vanish when the simulation period reaches 200 s and while the distributions of $q_{1,0}$, and $q_{0,1}$ increase and broaden, results obtained from the DWOSMC method agree well with those derived from SM.

Fig. 7   Particle volume density distributions of $q_{1,0}$ and $q_{0,1}$ for simulation times (a) $t = 60$ s and (b) $t = 200$ s obtained from the SM (solid line) and DWOSMC method (scattered solid points) for Case III.

3.2.3 Initially non-uniformly distributed and compositionally different volume case

The initial particles are initially exponentially distributed according to Eq. (24) [12], and the compositions of components A and B are different for Case IV. The initial total particle number is N_0 $=10^5$/m^3, and the initial average particle volume is $v_0 = 1\times10^{-22}$ m^3, in which the volumes of components A and B are $v_{A0}= v_0/3$, $v_{B0}= 2v_0/3$, respectively. Coagulation and condensation kernels used are the same as those used for Case II. A simulation period of 200 s is used.

$$n(v_{A},v_{B},0) = N_0/v_0\times\exp\left(-\frac{v(v_{A},v_{B},0)}{v_0}\right) \tag{24}$$

From Fig. 8(a) it is remarkable that dimensionless particle number density N/N_0 and total particle volume V/V_0 values obtained from the two methods (i.e., the SM and DWOSMC method) are in

16

excellent agreement with one another. The particle number distributions observed at simulation times $t = 20$ s and 200 s are shown in Fig. 8(b), and it should be noted that for the initially exponentially distributed case, the PSD for simulation time $t = 20$ s more closely reflects a normal distribution than it does for initially uniformly distributed Case II. Particles are normally distributed when the simulation time reaches 200 s. The results obtained from the DWOSMC method are in excellent agreement with those derived from SM.

Fig. 8   Time evolution of (a) N/N_0 and V/V_0 and (b) particle number distributions obtained from the SM (solid line) and DWOSMC method (scattered solid points) for Case IV.

The component related particle volume density distributions of $q_{1,0}$, and $q_{0,1}$ obtained over simulation periods $t = 20$ s and 200 s are shown in Fig. 9(a) and Fig. 9(b), respectively. It can be clearly observed that the particle volume density distributions of both components increase and grow broader, and that the difference between the particle volume density distributions of components A and B is pronounced. Particle volume density distributions obtained through the DWOSMC are consistent with those derived from the SM.

Fig. 9   Particle volume density distributions of $q_{1,0}$ and $q_{0,1}$ for simulation times (a) $t = 20$ s and (b) $t = 200$ s obtained from the SM (solid line) and DWOSMC method (scattered solid points) for Case IV.

3.3 Two-component coagulation and condensation process and the sum coagulation kernel case

The coagulation kernel is no longer constant and is written as $K = K_0(v_i + v_j)$ [48] for Case V. The initial particle size distribution satisfies a normal distribution according to Eq. (25), and the compositions of components A and B are different. The initial total particle number is $N_0 = 10^{11}/m^3$ and the initial average particle volume is $v_0 = \times 10^{-19}$ m^3, in which the volumes of components A and B are $v_{A0} = v_0/3$, $v_{B0} = 2v_0/3$, respectively. The standard deviation σ is 2×10^{-18} m^3. The linear condensation kernels for components A and B are given by $I_A = \sigma_A v_A$, $\sigma_A = 1 \times 10^{-3}$/s, $I_B = \sigma_B v_B$ and $\sigma_B = 2 \times 10^{-3}$/s, respectively. A simulation period of 100 s is used.

$$n(v_A, v_B, 0) \quad = \frac{N_0}{\sqrt{2\pi}\sigma} \times \exp\left(-\frac{(v(v_A, v_B, 0) - v_0)^2}{2\sigma^2}\right) \tag{25}$$

The time evolution of dimensionless particle number density N/N_0 and total particle volume V/V_0 and the particle number distribution of $q_{0,0}$ for simulation times 10 s and 100 s are shown in Fig. 10 for Case V. As was expected, for N/N_0 and V/V_0, results obtained from the DWOSMC and SM are in agreement with one another. For the particle size distribution shown in Fig. 10(b), as particles are initially normally distributed, when the simulation time reaches 10 s, the distribution of $q_{0,0}$ closely reflects a normal distribution. In contracts to patterns found from the other cases, the peak diameter of

17

particles almost remains at the same value for Case V. The results obtained from the SM and DWOSMC method are in excellent agreement with one another.

Fig. 10   Time evolution of (a) N/N_0 and V/V_0 and (b) particle number distributions obtained from the SM (solid line) and DWOSMC method (scattered solid points) for Case V.

Fig. 11 shows the particle volume density distributions of components A and B for the simulation times of 10 s and 100 s. From

Fig. 11 (a) and (b), while the peak diameter of the $q_{0,0}$ distribution does not change, the peak diameter of $q_{1,0}$ and $q_{0,1}$ tends to be larger. As the time period reaches 100 s, the distributions of $q_{1,0}$, and $q_{0,1}$ become broader and more closely reflect normal distributions. The results obtained from the DWOSMC method are in excellent agreement with those derived from the SM.

Fig. 11   Particle volume density distributions of (a) $q_{1,0}$ and (b) $q_{0,1}$ for simulation times t =10 s and t =100 s obtained from the SM (solid line) and DWOSMC method (scattered solid points) for Case V.

3.4 Two-component coagulation and condensation process and the free molecule regime case

Coagulation and condensation processes are considered to occur in a free molecule regime (where the diameter of particles is smaller than the mean free path of air) for Case VI. In the free molecule regime, the coagulation kernel is determined as [17],

$$K(v_i, v_j) = (\frac{6}{\pi})^{2/3}(\frac{\pi k_B T_K}{2\rho})^{1/2}(\frac{1}{v_i}+\frac{1}{v_j})^{1/2}(v_i^{1/3}+v_j^{1/3})^2 \qquad (26)$$

where v_i and v_j are the volumes of two coagulated particles i and j, respectively, and T_K is temperature, k_B is Boltzmann's constant and ρ is the density of particles.

The initial particle size distribution satisfies a normal distribution in Eq. (25), and the compositions of components A and B are different. The initial total particle number is $N_0 = 10^{12}/m^3$ and the initial average particle volume is $v_0 = 3\times10^{-18}$ m^3, in which the volumes of components A and B are $v_{A0} = v_0/3$ and $v_{B0} = 2v_0/3$, respectively. The standard deviation σ is 1×10^{-18} m^3. The linear condensation kernels of components A and B are given by $I_A = \sigma_A v_A$, $\sigma_A = 1\times10^{-3}$/s, $I_B = \sigma_B v_B$ and $\sigma_B = 2\times10^{-3}$/s, respectively. A simulation period of 100 s is used.

Fig. 12 shows the time evolution of dimensionless particle number density N/N_0 and total particle volume V/V_0 as well as the particle number distribution of $q_{0,0}$ for Case VI. For N/N_0 and V/V_0, results

18

obtained from the DWOSMC method and SM are in excellent agreement with one another as shown in Fig. 12(a). From Fig. 12(b), the distribution curve of $q_{0,0}$ is steep and narrow for a simulation period of 10 s, and the distribution curve of $q_{0,0}$ is broader and much more gradual as the simulation time reaches 100 s. At a simulation time of 10 s, some fluctuations are observed at a peak value of $q_{0,0}$. However, when the simulation time reaches 100 s, the peak diameter of $q_{0,0}$ is larger, the distribution of $q_{0,0}$ is normal with slight fluctuations, and results obtained from the DWOSMC method and SM agree well with one another.

Fig. 12   Time evolution of (a) N/N_0 and V/V_0 and (b) particle number distributions obtained from the SM (solid line) and DWOSMC method (scattered solid points) for Case VI.

Fig. 13 shows the particle volume density distributions for components A and B for simulation times of 10 s and 100 s. Fig. 13(a) shows that the distribution of $q_{1,0}$ tends to be broader and that the peak diameter of $q_{1,0}$ is larger. Similar variations are found for component B as shown in Fig. 13(b), though the value of $q_{0,1}$ is larger than $q_{1,0}$ due to the use of different condensation kernels for components A and B. The distributions of $q_{1,0}$ and $q_{0,1}$ obtained from the DWOSMC method and SM agree well with one another.

Fig. 13   Particle volume density distributions of (a) $q_{1,0}$ and (b) $q_{0,1}$ for simulation times t= 10 s and 100 s obtained from the SM (solid line) and DWOSMC method (scattered solid points) for Case VI.

The normalized combined number density distribution of A-component and B-component (i.e., the bivariate compositional distribution) is defined as follows,

$$n_\mathrm{d}=100n(v_\mathrm{A},v_\mathrm{B},t)/N_0 \tag{27}$$

In Case VI, bivariate compositional distributions for different simulation times t are shown in Fig. 14. The contour plot of the normalized bivariate compositional distribution function is mostly positioned in the diagonal area based on the dimensionless coordinates of v_A/v_0 and v_B/v_0. As simulation time increases from $t = 20$ s to $t = 100$ s, the normalized bivariate compositional distribution function tends to be smaller but distributed across a larger region with respect to compositional particle volumes.

Fig. 14   Dimensionless bivariate compositional distributions observed at different simulation times t obtained from the DWOSMC method for Case VI.

3.5 Computational Accuracy and Efficiency Analysis

To evaluate the computational accuracy and efficiency of the multi-component DWOSMC method proposed in the present study, the calculated relative error ε (%) according to Eq. (19) (here $A_0(t)$ is the value obtained from the sectional method) is shown in Fig. 15; the normalized computational time τ according to Eq. (20) (i.e., the reference value is the computational time of Case I derived from the SM) for the studied cases is listed in Table 1. In Fig. 15, maximum relative errors range within 0.8% for Cases I to IV and 1.2% for Cases V and VI, respectively, showing that even in complex two-component systems involving coagulation and condensation processes, the newly developed DWOSMC method is computationally accurate and relative errors generated are very small. In addition, relative errors obtained from two-component Cases II to VI do not tend to be significantly larger than those of one-component Case I. Furthermore, it is well known that the SM is generally more computationally powerful than the MC method for one-component systems (e.g., for Case I). When the two methods are further extended to consider two-components, Table 1 shows that τ of the DWOSMC method generates much smaller values than the SM for most of the two-component cases. This is the case because when considering more component information, the programming algorithm for the SM correspondingly becomes more complex while the MC method does not. Hence, it is concluded that the proposed multi-component DWOSMC method is superior to the SM in terms of its computational efficiency in addressing multi-component problems.

Fig. 15   Time evolution of the relative error ε (%) for N/N_0 obtained from the DWOSMC method for different cases.

Table 1.   Normalized computational time τ derived from different cases using the SM and DWOSMC method.

4 Conclusions

A newly modified differentially weighted operator splitting Monte Carlo (DWOSMC) method is developed to simulate two-component aerosol dynamics in the present study. Compared to traditional MC methods, the multi-component DWOSMC method proposed in the present study adopts "different weights" which is more suitable for obtaining the compositional distributions of particles, especially for multi-component systems. In addition, the operator splitting technique renders it applicable and more efficient to couple the stochastic MC method with the deterministic integration method.

Different initial size distribution functions and initial compositional distributions are studied under various regimes of simultaneous aerosol coagulation and condensation that include three cases involving constant coagulation kernel, one case involving sum coagulation kernel and one case involving free molecule coagulation kernel. For all of these cases studied, dimensionless particle

number density, total particle volume, and component related particle volume density distributions are examined, and results obtained from the DWOSMC method agree well with those derived from the SM.

The present results and findings show that the multi-component DWOSMC method is more computationally accurate and efficient than traditional non-weighted MC methods. Furthermore, the SM is more computationally efficient than the DWOSMC when applied to one-component aerosol simulation systems while the DWOSMC tends to be more computationally efficient when applied to two-component aerosol simulation systems. This is the case because considering more than one form of component information does not significantly increase the complexity of the MC algorithm while much higher levels of complexity are required to use the SM algorithm to simulate more than one component of aerosol dynamics. With such high levels of computational efficiency and accuracy based on the specific data and evidence obtained, the newly developed multi-component DWOSMC method cannot only predict particle size distributions, but can also determine component-related particle volume density and bivariate compositional distributions.

Acknowledgements

References

[1]   C.E.Kolb, D.R.Worsnop, Chemistry and composition of atmospheric aerosol particles, Annu. Rev. Phys. Chem. 63 (2012) 471–491.

[2]   D.Fino, S.Bensaid, M.Piumetti, N.Russo, A review on the catalytic combustion of soot in diesel particulate filters for automotive applications: From powder catalysts to structured reactors, Appl. Catal. A Gen. 509 (2016) 75–96.

[3]   J.Fang, Y.Wang, J.Kangasluoma, M.Attoui, H.Junninen, M.Kulmala, T.Petäjä, P.Biswas, The initial stages of multicomponent particle formation during the gas phase combustion synthesis of mixed SiO2/TiO2, Aerosol Sci. Technol. 52 (2018) 277–286.

[4]   U.Pöschl, Atmospheric aerosols: Composition, transformation, climate and health effects, Atmos. Chem. 44 (2005) 7520–7540.

[5]   H.Korhonen, K.E.J.Lehtinen, M.Kulmala, Multicomponent aerosol dynamics model UHMA: model development and validation, Atmos. Chem. Phys. 4 (2004) 757–771.

[6]   F.Gelbard, J.H.Seinfeld, Simulation of multicomponent aerosol dynamics, J. Colloid Interface Sci. 78 (1980) 485–501.

[7]   S.Simons, The condensation,coagulation and deposition of a multicomponent radioactive aerosol., Ann. Nucl. Energy. 9 (1982) 473–479.

[8]   A.Prakash, A.P.Bapat, M.R.Zachariah, A simple numerical algorithm and software for solution of nucleation, surface growth, and coagulation problems, Aerosol Sci. Technol. 37 (2003) 892–898.

[9]   Z.Haibo, Z.Chuguang, X.Minghou, Multi-Monte Carlo approach for general dynamic equation considering simultaneous particle coagulation and breakage, Powder Technol. 154 (2005) 164–178.

[10]   S.Y.Liu, T.L.Chan, A coupled CFD-Monte Carlo method for simulating complex aerosol dynamics in turbulent flows, Aerosol Sci. Technol. 51 (2017) 269–281.

[11]   T.E.Ramabhadran, T.W.Peterson, J.H.Seinfeld, Dynamics of aerosol coagulation and condensation, AIChE J. 22 (1976) 840–851.

[12]   H.Zhao, C.Zheng, M.Xu, Multi-Monte Carlo method for coagulation and condensation/evaporation in dispersed systems, J. Colloid Interface Sci. 286 (2005) 195–208.

[13]   K.Fu, D.Liang, W.Wang, M.Cui, The time second-order characteristic FEM for nonlinear multicomponent aerosol dynamic equations in environment, Int. J. Numer. Anal. Model. 12 (2015) 211–229.

[14]   C.Housiadas, Y.Drossinos, Aerosol Flows, Mech. Eng. CRC Press. (2005).

[15]   S.K.Friedlander, Smoke, dust and haze: fundamentals of aerosol, Oxford University Press, New York, 2000.

[16]   A.Maisels, F.Einar Kruis, H.Fissan, Direct simulation Monte Carlo for simultaneous nucleation, coagulation, and surface growth in dispersed systems, Chem. Eng. Sci. 59 (2004) 2231–2239.

[17]   K.Zhou, Z.He, M.Xiao, Z.Zhang, Parallel Monte Carlo simulation of aerosol dynamics, Adv. Mech. Eng. 6 (2014) 1–11.

[18]   S.Y.Liu, T.L.Chan, A stochastically weighted operator splitting Monte Carlo (SWOSMC) method for the numerical simulation of complex aerosol dynamic processes, Int. J. Numer. Methods Heat Fluid Flow. 27 (2017) 263–278.

[19]   Z.Wan, Z.You, J.Chen, M.Wang, Modeling of aggregation kinetics by a new moment method, Appl. Math. Model. 39 (2015) 6915–6924.

[20]   F.Gelbard, Modeling multicomponent aerosol particle growth by vapor condensation, Aerosol Sci. Technol. 12 (1990) 399–412.

[21]   Y.P.Kim, J.H.Seinfeld, Simulation of multicomponent aerosol condensation by the moving sectional method, J. Colloid Interface Sci. 135 (1990) 185–199.

[22]   Y.P.Kim, Simulation of multicomponent aerosol dynamics, J. Colloid Interface Sci. 149 (1992) 425–449.

[23]   D.Katoshevski, J.H.Seinfeld, Analytical solution of the multicomponent aerosol general dynamic equation — without Coagulation, Aerosol Sci. Technol. 27 (1997) 541–549.

[24] D.Katoshevski, J.H.Seinfeld, Analytical–numerical solution of the multicomponent aerosol general dynamic equation—with coagulation, Aerosol Sci. Technol. 27 (1997) 550–556.

[25] Z.Sun, R.Axelbaum, J.Huertas, Monte Carlo simulation of multicomponent aerosols undergoing simultaneous coagulation and condensation, Aerosol Sci. Technol. 38 (2004) 963–971.

[26] Z.Sun, R.L.Axelbaum, B.H.Chao, A multicomponent sectional model applied to flame synthesis of nanoparticles, Proc. Combust. Inst. 29 (2002) 1063–1069.

[27] T.Matsoukas, T.Kim, K.Lee, Bicomponent aggregation with composition-dependent rates and the approach to well-mixed state, Chem. Eng. 64 (2009) 787–799.

[28] Y.Efendiev, Modeling and simulation of multi-component aerosol dynamics, Comput. Appl. Math. 23 (2004) 401–423.

[29] H.Zhao, C.Zheng, Two-component brownian coagulation: Monte carlo simulation and process characterization, Particuology. 9 (2011) 414–423.

[30] T.Matsoukas, K.Lee, T.Kim, Mixing of components in two-component aggregation, AIChE J. 52 (2006) 3088–3099.

[31] K.Lee, T.Kim, P.Rajniak, T.Matsoukas, Compositional distributions in multicomponent aggregation, Chem. Eng. Sci. 63 (2008) 1293–1303.

[32] H.Zhao, F.E.Kruis, C.Zheng, Monte carlo simulation for aggregative mixing of nanoparticles in two-component systems, Ind. Eng. Chem. Res. 50 (2011) 10652–10664.

[33] H.Zhao, Z.Xu, H.Zhao, Predictions on dynamic evolution of compositional mixing degree in two-component aggregation, J. Aerosol Sci. 101 (2016) 10–21.

[34] H.Zhao, F.E.Kruis, Dependence of steady-state compositional mixing degree on feeding conditions in two-component aggregation, Ind. Eng. Chem. Res. 53 (2014) 6047–6055.

[35] G.Palaniswaamy, DSMC multicomponent aerosol dynamics: sampling algorithms and aerosol processes, University of Missouri-Columbia, 2007.

[36] F.Gelbard, J.H.Seinfeld, Coagulation and growth of a multicomponent aerosol, J. Colloid Interface Sci. 63 (1978) 472–479.

[37] T.L.Chan, Y.H.Liu, C.K.Chan, Direct quadrature method of moments for the exhaust particle formation and evolution in the wake of the studied ground vehicle, J. Aerosol Sci. 41 (2010) 553–568.

[38] T.L.Chan, S.Y.Liu, Y.Yue, Nanoparticle formation and growth in turbulent flows using the bimodal TEMOM, Powder Technol. 323 (2017) 507–517.

[39] M.Yu, J.Lin, Hybrid method of moments with interpolation closure – Taylor-series expansion method of moments scheme for solving the Smoluchowski coagulation equation, Appl. Math. Model. 52 (2017) 94–106.

[40] M.Yu, Y.Liu, G.Jin, H.Jin, A new analytical solution for agglomerate growth undergoing Brownian coagulation, Appl. Math. Model. 40 (2016) 5497–5509.

[41] N.Metropolis, S.Ulam, The Monte Carlo Method, J. Am. Stat. Assoc. 44 (1949) 335–341.

[42] G.A.Bird, Molecular gas dynamics, in: NASA STI/Recon Tech. Rep. A 76, Clarendon Press, Oxford, 1976.

[43] G.A.Bird, Molecular gas dynamics and the direct simulation of gas flows, Clarendon Press, New York, 1994.

[44] H.Zhao, C.Zheng, Correcting the multi-Monte Carlo method for particle coagulation, Powder Technol. 193 (2009) 120–123.

[45] J.Wei, F.E.Kruis, A GPU-based parallelized Monte-Carlo method for particle coagulation using an acceptance-rejection strategy, Chem. Eng. Sci. 104 (2013) 451–459.

[46] S.Rjasanow, A Stochastic Weighted Particle Method for the Boltzmann Equation, J. Comput. Phys. 124 (1996) 243–253.

[47] R.I.A.Patterson, W.Wagner, M.Kraft, Stochastic weighted particle methods for population balance equations, J. Comput. Phys. 230 (2011) 7456–7472.

[48] H.Zhao, F.E.Kruis, C.Zheng, A differentially weighted Monte Carlo method for two-component coagulation, J. Comput. Phys. 229 (2010) 6931–6945.

[49] M.Celnik, R.Patterson, M.Kraft, W.Wagner, Coupling a stochastic soot population balance to gas-phase chemistry using operator splitting, Combust. Flame. 148 (2007) 158–176.

[50] W.J.Menz, J.Akroyd, M.Kraft, Stochastic solution of population balance equations for reactor networks, J. Comput. Phys. 256 (2014) 615–629.

[51] H.M.Liu, T.L.Chan, A new differentially weighted operator splitting Monte Carlo method for aerosol dynamics., in: Proc. 24th Int. Conf. Model. Monit. Manag. Air Pollut. (Air Pollut. 2016), June 20-22, 2016, Crete, Greece., 2016: pp. 237–248.

[52] H.M.Liu, T.L.Chan, Differentially weighted operator splitting Monte Carlo method for simulating complex aerosol dynamic processes, Particuology. 36 (2018) 114–126.

[53] H.Zhao, F.E.Kruis, C.Zheng, Reducing statistical noise and extending the size spectrum by applying weighted simulation particles in Monte Carlo simulation of doagulation, Aerosol Sci. Technol. 43 (2009) 781–793.

[54] Z.Xu, H.Zhao, C.Zheng, Fast Monte Carlo simulation for particle coagulation in population balance, J. Aerosol Sci. 74 (2014) 11–25.

[55] G.Palaniswaamy, S.K.Loyalka, Direct simulation, Monte Carlo, aerosol dynamics: Coagulation and condensation, Ann. Nucl. Energy. 35 (2008) 485–494.

[56] K.Liffman, A direct simulation Monte-Carlo method for cluster coagulation, J. Comput. Phys. 100 (1992) 116–127.

[57] F.Gelbard, Y.Tambour, J.H.Seinfeld, Sectional representations for simulating aerosol dynamics, J. Colloid Interface Sci. 76 (1980) 541–556.

[58] A.Sandu, Piecewise polynomial solutions of aerosol dynamic equation, Aerosol Sci. Technol. 40 (2006) 261–273.
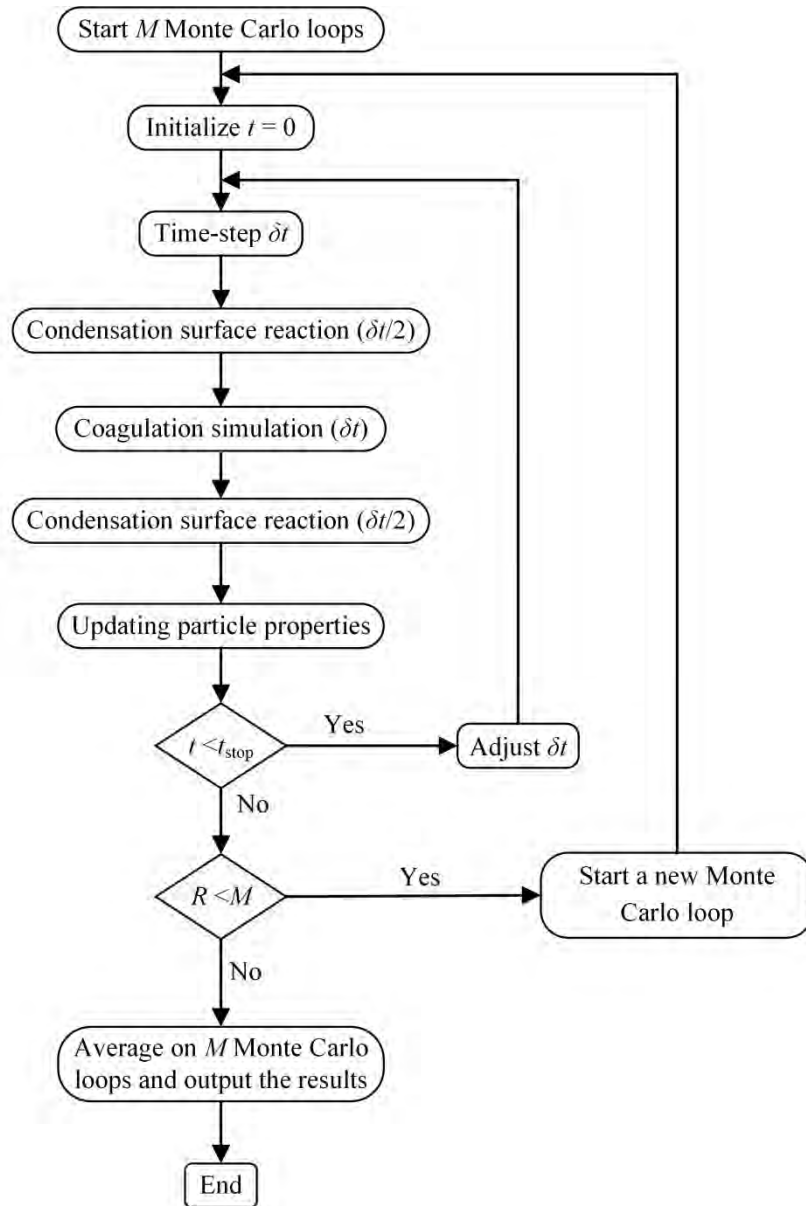
List of Figures

Fig. 1   Flowchart of the two-component DWOSMC algorithm.

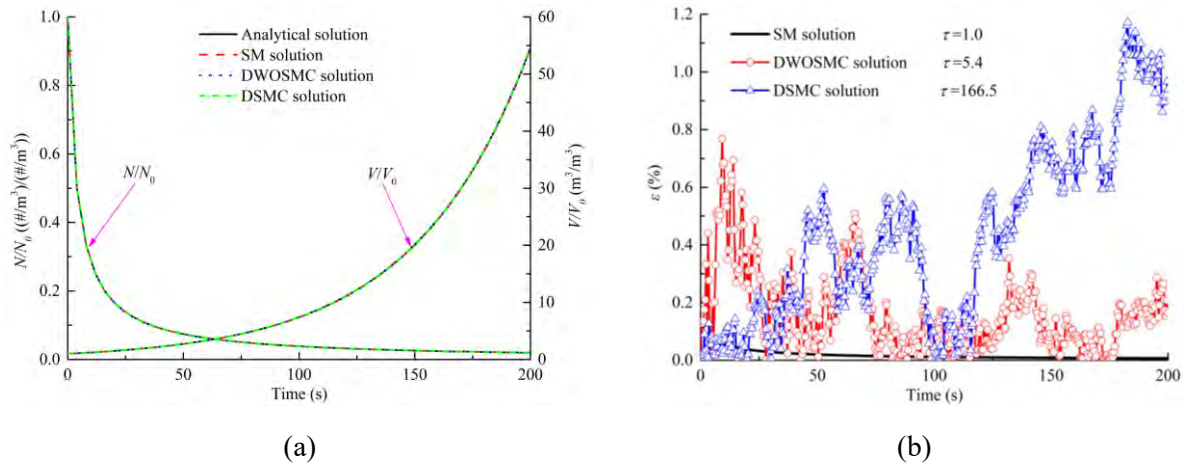Fig. 2   Time evolution of (a) dimensionless particle number concentration N/N_0 and total particle volume V/V_0 ; and (b) the relative error ε (%) for N/N_0 obtained from the SM, DWOSMC and DSMC methods, and the corresponding normalized computation time τ, for Case I.
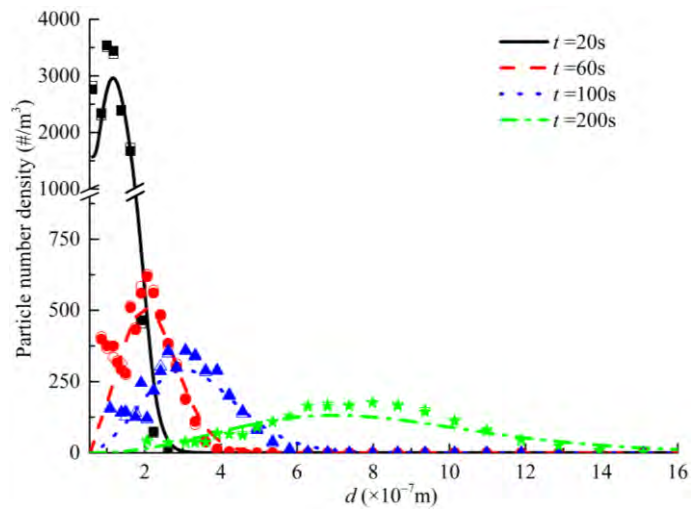
Fig. 3   Evolution of particle number distributions obtained from the sectional (solid line), DWOSMC (scattered solid points) and DSMC (scattered unshaded points) methods for Case I.
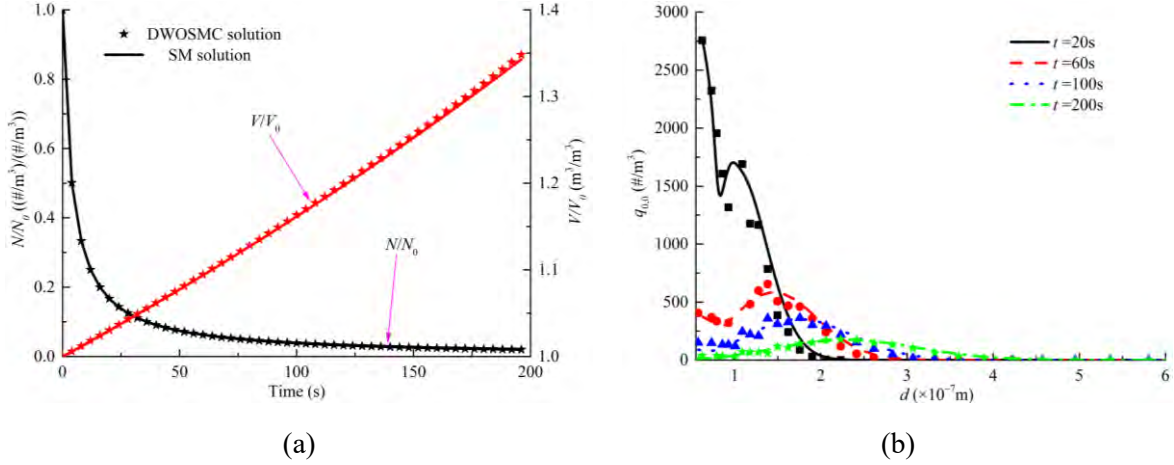
Fig. 4   Time evolutions of (a) N/N_0 and V/V_0 and (b) particle number distributions obtained from the SM (solid line) and DWOSMC method (scattered solid points) for Case II.
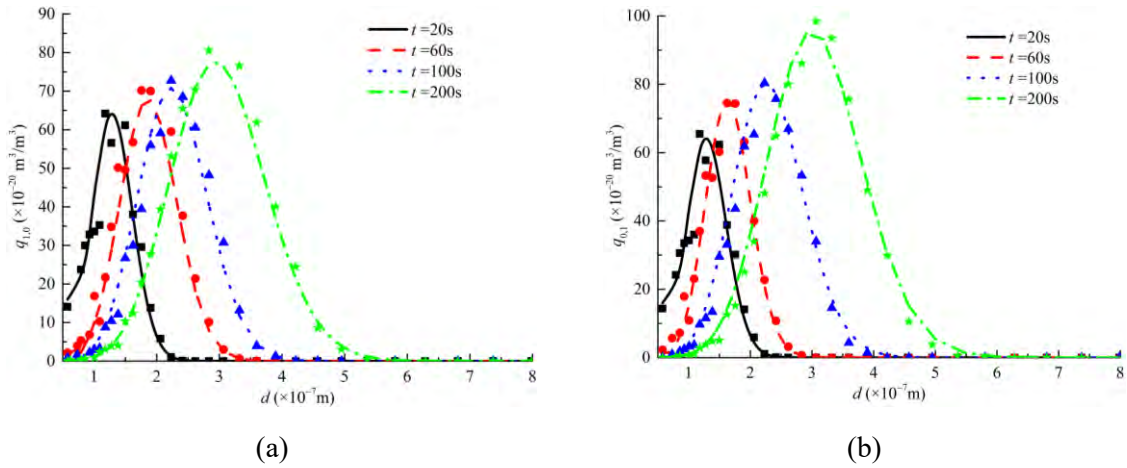
Fig. 5   Time evolutions of particle volume density distributions of (a) A-component and (b) B-component obtained from the SM (solid line) and DWOSMC method (scattered solid points) for Case II.

Fig. 6   Time evolution of (a) N/N_0 and V/V_0 and (b) particle number distributions obtained from the SM (solid line) and DWOSMC method (scattered solid points) for Case III.

Fig. 7   Particle volume density distributions of $q_{1,0}$ and $q_{0,1}$ for simulation times (a) $t = 60$ s and (b) $t = 200$ s obtained from the SM (solid line) and DWOSMC method (scattered solid points) for Case III.

Fig. 8   Time evolution of (a) N/N_0 and V/V_0 and (b) particle number distributions obtained from the SM (solid line) and DWOSMC method (scattered solid points) for Case IV.

Fig. 9   Particle volume density distributions of $q_{1,0}$ and $q_{0,1}$ for simulation times (a) $t = 20$ s and (b) $t = 200$ s obtained from the SM (solid line) and DWOSMC method (scattered solid points) for Case IV.

Fig. 10   Time evolution of (a) N/N_0 and V/V_0 and (b) particle number distributions obtained from the SM (solid line) and DWOSMC (scattered solid points) for Case V.

Fig. 11   Particle volume density distributions of (a) $q_{1,0}$ and (b) $q_{0,1}$ for simulation times $t =10$ s and $t =100$ s obtained from the SM (solid line) and DWOSMC method (scattered solid points) for Case V.
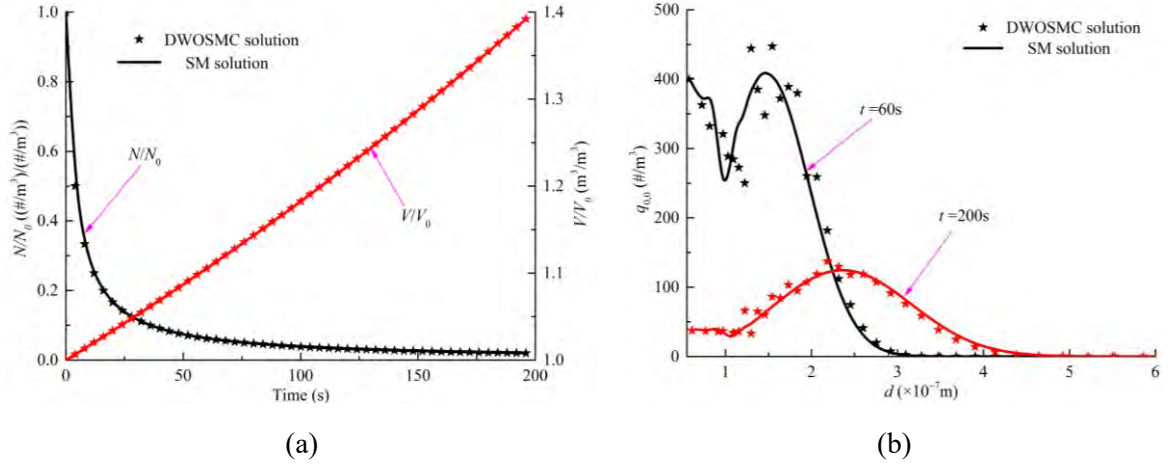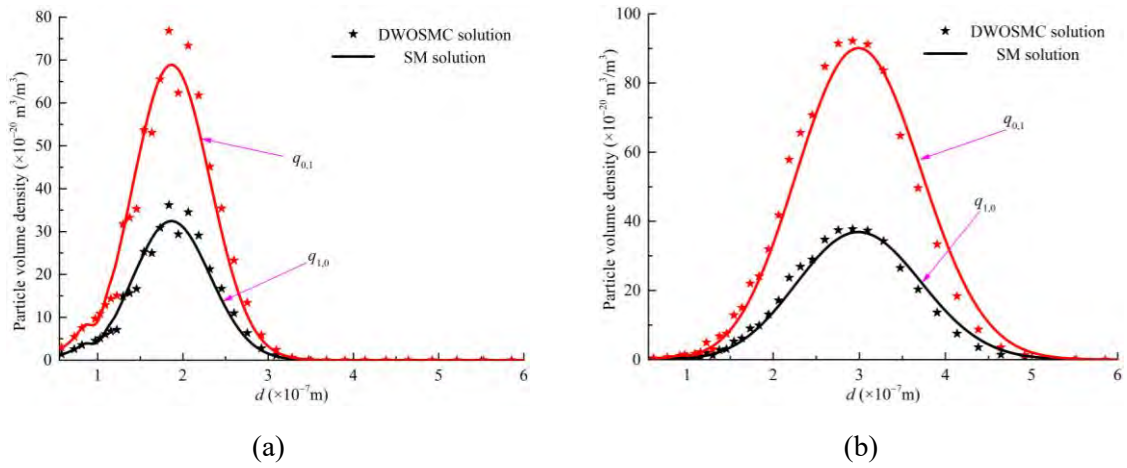
Fig. 12   Time evolution of (a) N/N_0 and V/V_0 and (b) particle number distributions obtained from the SM (solid line) and DWOSMC method (scattered solid points) for Case VI.

Fig. 13   Particle volume density distributions of (a) $q_{1,0}$ and (b) $q_{0,1}$ over simulation times $t=10$ s and 100 s obtained from the SM (solid line) and DWOSMC method (scattered solid points) for Case VI.

Fig. 14   Dimensionless bivariate compositional distributions observed at different simulation times t obtained from the DWOSMC method for Case VI.

Fig. 15   Time evolution of the relative error ε (%) for N/N_0 obtained from the DWOSMC method for different cases.

Fig. 1 Flowchart of the two-component DWOSMC algorithm.

Fig. 2　Time evolution of (a) dimensionless particle number concentration N/N_0 and total particle volume V/V_0 ; and (b) the relative error ε (%) for N/N_0 obtained from the SM, DWOSMC and DSMC methods, and the corresponding normalized computation time τ, for Case I.

Fig. 3　Evolution of particle number distributions obtained from the sectional (solid line), DWOSMC (scattered solid points) and DSMC (scattered unshaded points) methods for Case I.

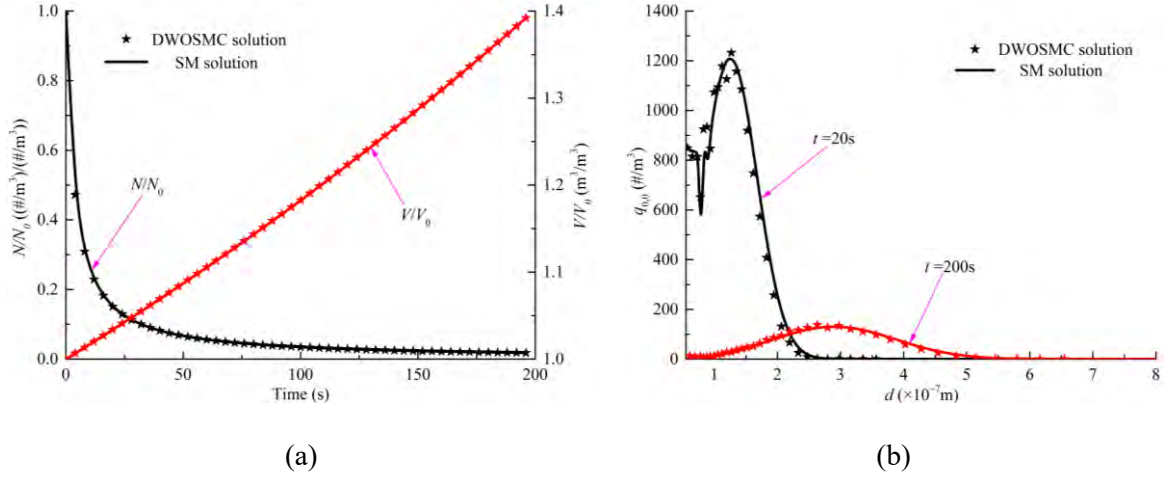(a)   (b)

Fig. 4   Time evolutions of (a) N/N_0 and V/V_0 and (b) particle number distributions obtained from the SM (solid line) and DWOSMC method (scattered solid points) for Case II.

(a)   (b)

Fig. 5   Time evolutions of particle volume density distributions of (a) A-component and (b) B-component obtained from the SM (solid line) and DWOSMC method (scattered solid points) for Case II.

Fig. 6   Time evolution of (a) N/N_0 and V/V_0 and (b) particle number distributions obtained from the SM (solid line) and DWOSMC (scattered solid points) for Case III.
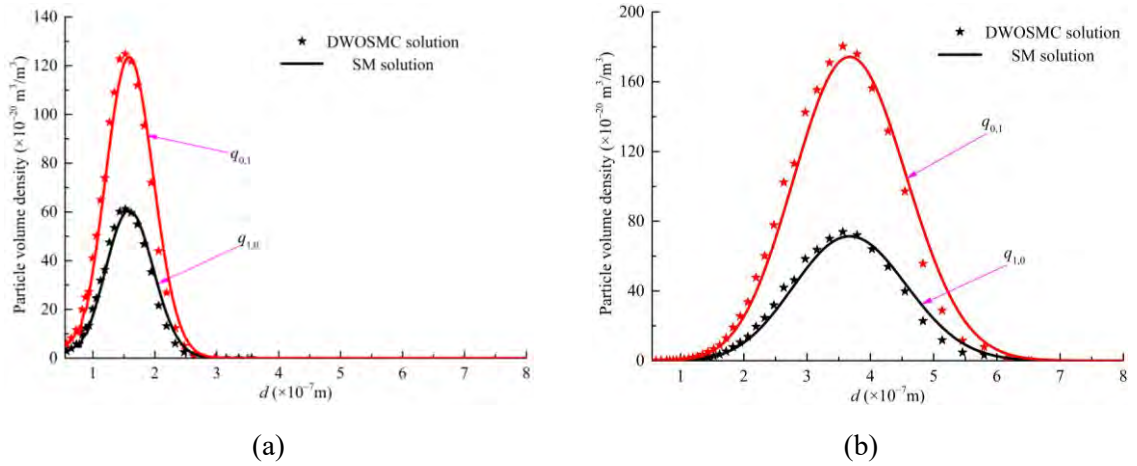

Fig. 7   Particle volume density distributions of $q_{1,0}$ and $q_{0,1}$ for simulation times (a) $t = 60$ s and (b) $t = 200$ s obtained from the SM (solid line) and DWOSMC method (scattered solid points) for Case III.
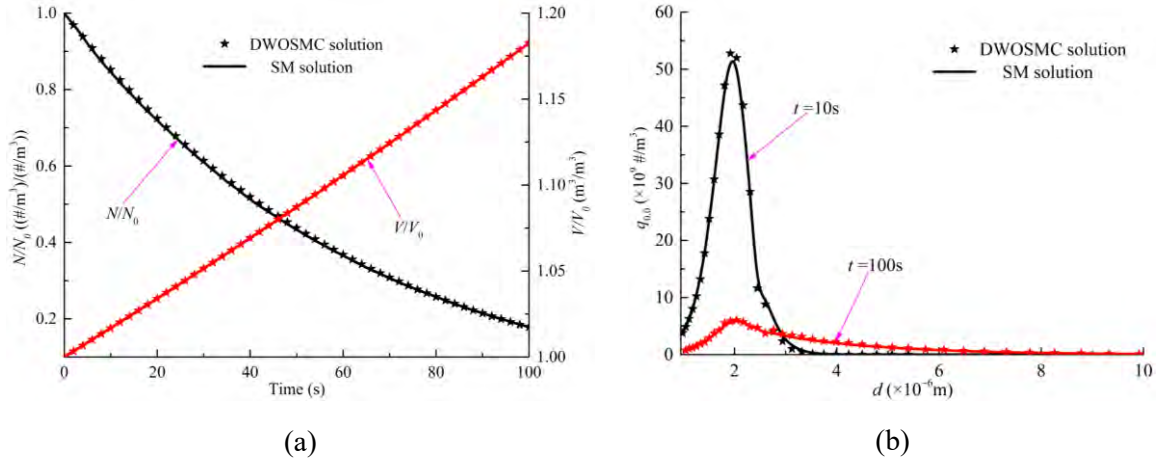
Fig. 8   Time evolution of (a) N/N_0 and V/V_0 and (b) particle number distributions obtained from the SM (solid line) and DWOSMC method (scattered solid points) for Case IV.
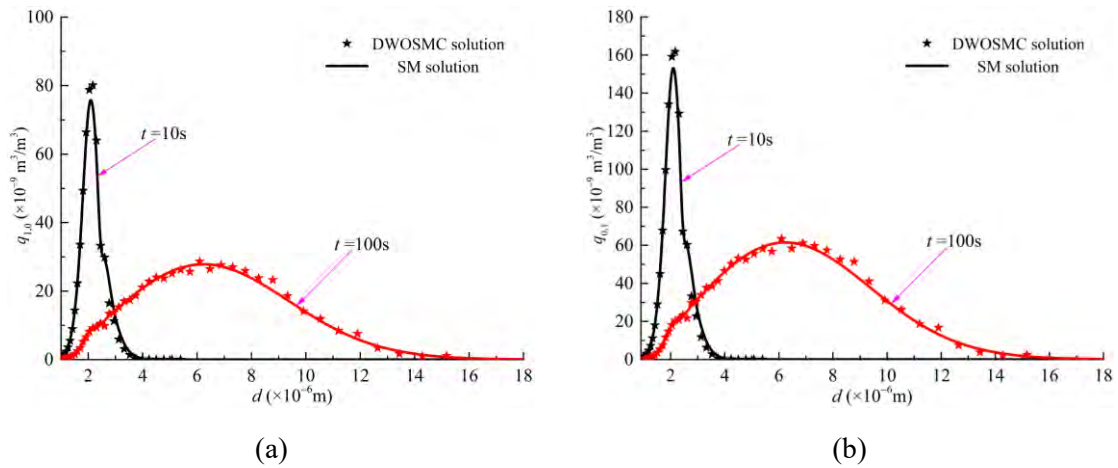

Fig. 9   Particle volume density distributions of $q_{1,0}$ and $q_{0,1}$ for simulation times (a) t = 20 s and (b) t = 200 s obtained from the SM (solid line) and DWOSMC method (scattered solid points) for Case IV.

Fig. 10   Time evolution of (a) N/N_0 and V/V_0 and (b) particle number distributions obtained from the SM (solid line) and DWOSMC method (scattered solid points) for Case V.

Fig. 11   Particle volume density distributions of (a) $q_{1,0}$ and (b) $q_{0,1}$ for simulation times $t = 10$ s and $t = 100$ s obtained from the SM (solid line) and DWOSMC method (scattered solid points) for Case V.
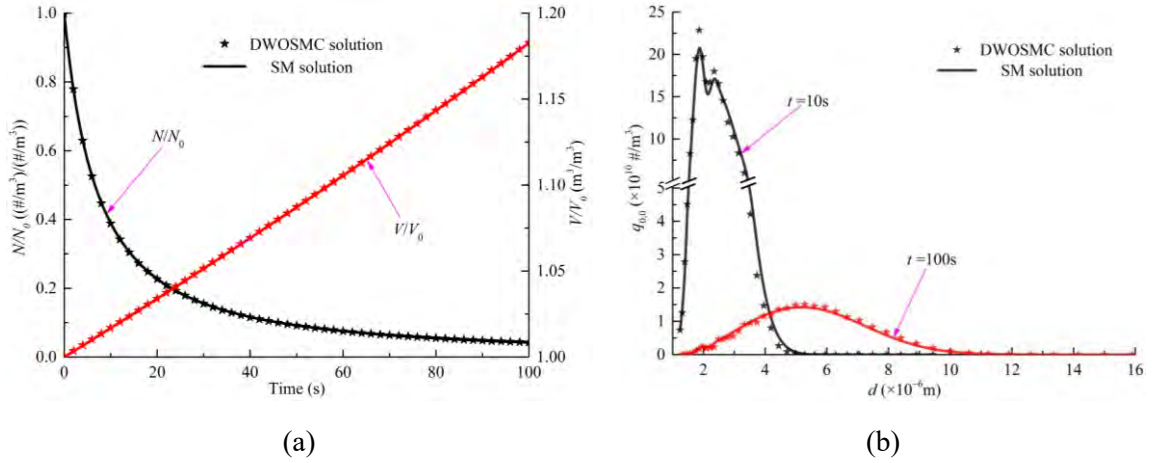
Fig. 12   Time evolution of (a) N/N_0 and V/V_0 and (b) particle number distributions obtained from the SM (solid line) and DWOSMC method (scattered solid points) for Case VI.
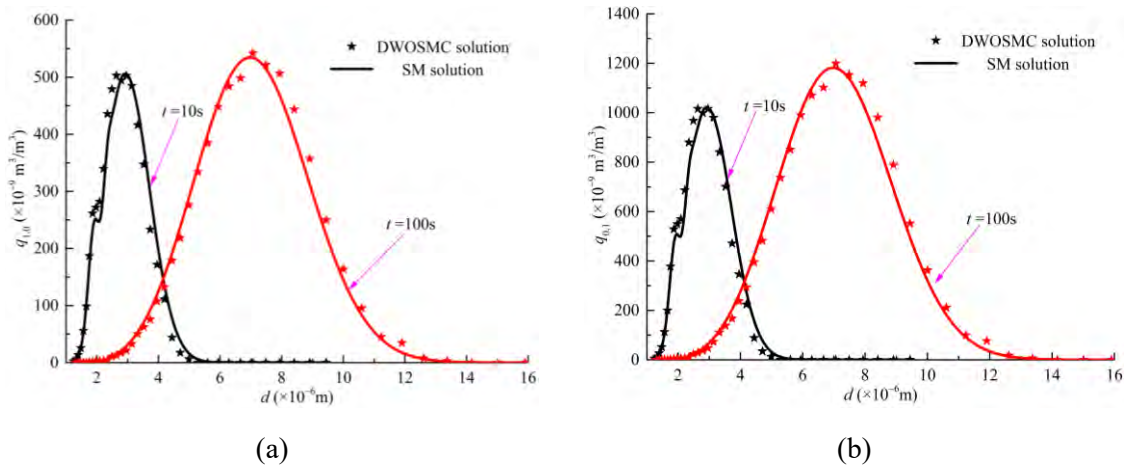

Fig. 13   Particle volume density distributions of (a) $q_{1,0}$ and (b) $q_{0,1}$ over simulation time t=10s and 100 s obtained from the SM (solid line) and DWOSMC method (scattered solid points) for Case VI.

(a)   (b)
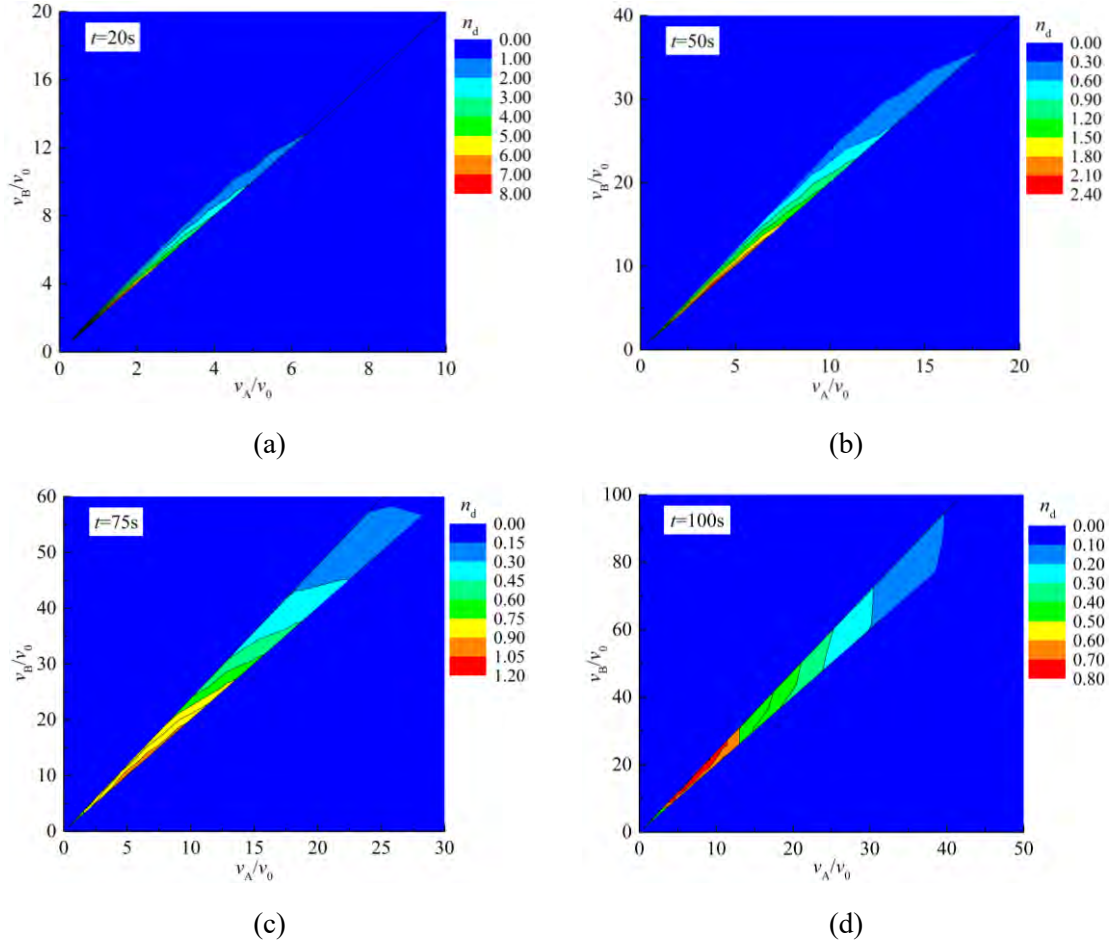
(c)   (d)

Fig. 14   Dimensionless bivariate compositional distributions observed at different simulation times obtained from the DWOSMC method for Case VI.
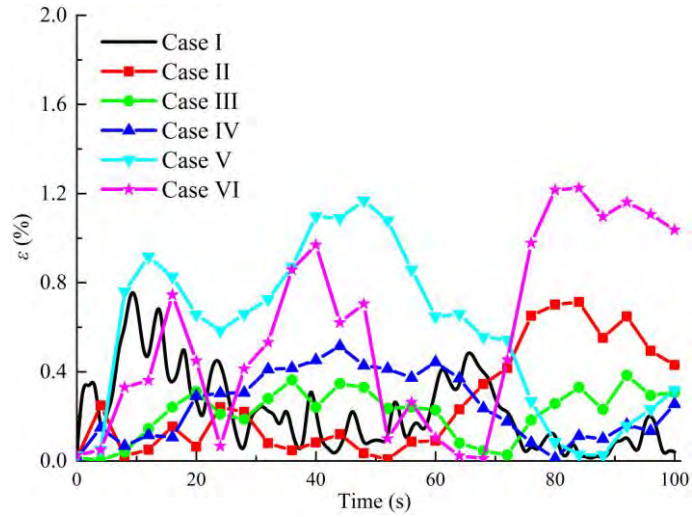

Fig. 15   Time evolution of the relative error ε (%) for N/N_0 obtained from the DWOSMC method for different cases.

List of Table

τ / Case	Methods	
	SM	DWOSMC
I	1.0	5.4
II	63.5	22.4
III	101.0	24.2
IV	115.1	24.4
V	177.2	25.5
VI	190.1	28.7

Table 1. Normalized computational time τ derived from different cases using the SM and DWOSMC method.